HHS Public Access

Author manuscript

Nat Methods. Author manuscript; available in PMC 2019 April 10.

Published in final edited form as:

Nat Methods. 2018 July ; 15(7): 523–526. doi:10.1038/s41592-018-0041-z.

StaPLs: versatile genetically encoded modules for engineering drug-inducible proteins

Conor L. Jacobs[1,3,4], **Ryan K. Badiee**[2,3,4,*], and **Michael Z. Lin**[3,4,5]

[1]Graduate Program in Biological Sciences, Stanford University, Stanford, California

[2]Department of Biology, Stanford University, Stanford, California

[3]Department of Neurobiology, Stanford University, Stanford, California

[4]Department of Bioengineering, Stanford University, Stanford, California

[5]Department of Pediatrics, Stanford University, Stanford, California

Abstract

Robust approaches for chemogenetic control of protein function would enable many biological applications. We describe stabilizable polypeptide linkages (StaPLs) based on hepatitis C virus protease. StaPLs undergo autoproteolysis to cleave proteins by default, while protease inhibitors prevent cleavage and preserve protein function. We created StaPLs responsive to different clinically approved drugs to bidirectionally control transcription with zinc-finger-based effectors, and used StaPLs to create single-chain drug-stabilizable variants of CRISPR/Cas9 and caspase-9.

Generalizable methods for pharmacological induction of protein function would be highly useful for gene- or cell-based therapies, or for investigating temporal requirements for proteins in biological systems. Existing methods include fusing proteins to steroid hormone-binding domains for sequestration in heat-shock complexes until drug application[1], fusing proteins to domains whose stability is enhanced by drug[2], and fusing complementary fragments to domains whose heterodimerization is induced by drug[2]. However, regulation by hormone-binding domains is not broadly generalizable[1], destabilization domains often allow some protein function in the absence of drug[3,4], and protein fragments often require optimization to suppress spontaneous reconstitution or obtain satisfactory drug-induced reconstitution[5,6]. Furthermore, fragment complementation requires two polypeptides for

Correspondence should be addressed to M.Z.L. (mzlin@stanford.edu).

*Present address: MD Program, UCSF School of Medicine, San Francisco, California

Author Contributions

M.Z.L. conceived of the study. C.L.J. designed orthogonal StaPL modules and StaPL-controlled proteins. R.K.B. and C.L.J. constructed plasmids, and C.L.J and R.K.B. designed and carried out mammalian cell experiments. M.Z.L. and C.L.J. wrote the manuscript, with contributions from R.K.B.

Competing Interests

M.Z.L., C.L.J., and R.K.B. have filed a provisional patent with the US Patent and Trademark Office for compositions and methods for inducing protein function.

each activity to be regulated, making simultaneous regulation of multiple activities cumbersome.

We sought to develop single-chain drug-controllable proteins whose function could be robustly activated by clinically available drugs that lack endogenous targets. Previously, we used the hepatitis C virus (HCV) nonstructural protein 3 protease domain (hereafter, NS3 protease) and its inhibitors[7] for drug-controlled protein tagging. In TimeSTAMP, a *cis*-cleaving NS3 protease removes a visualizable tag from a protein by default, but inhibitor application preserves the tag on newly synthesized copies[8,9]. In SMASh, removal of a degron from a protein by a *cis*-cleaving NS3 protease can be inhibited by drug, thus shutting off further protein production[10]. Consequently, we reasoned that an internal autoproteolytic module, comprising NS3 protease and a substrate sequence, would constitute a stabilizable polypeptide linkage (StaPL) that could control protein function in multiple ways (Fig. 1a). A StaPL module could link a protein to a functional domain, so that function is removed in the absence of inhibitor but retained in its presence. Alternatively, a StaPL module could be inserted within a domain so that the domain is cleaved into two fragments by default but remains intact in the presence of inhibitor. Finally, a StaPL module could be placed between two copies of a dimerization-activated protein, so that inhibitor preserves subsequently synthesized molecules as tandem dimers, leading to activation.

As controlling two processes in the same cell independently would be desirable, we first created two NS3 protease variants inhibited by different drugs, asunaprevir (ASV) and telaprevir (TPV), thus diverging NS3 into two species defined by drug sensitivity (Supplementary Note 1, Supplementary Table 1, Supplementary Fig. 1). These two variants, denoted $NS3^{AI}$ (ASV-inhibited) and $NS3^{TI}$ (TPV-inhibited), were orthogonal in their drug sensitivity, with $NS3^{AI}$ highly resistant to 1-10 μM TPV and $NS3^{TI}$ highly resistant to 0.1-1 μM ASV (Supplementary Fig. 2a-c). SMASh tags containing $NS3^{AI}$ or $NS3^{TI}$ (Supplementary Fig. 2d) allowed ASV or TPV, respectively, to suppress accumulation of fused YFP (Fig. 1b). Together, they allowed for simultaneous independent suppression of two protein targets (Fig. 1c), demonstrating that $NS3^{AI}$-ASV and $NS3^{TI}$-TPV are indeed orthogonal protease-inhibitor pairs. We next explored the possibility of regulating the linkage of other functional domains in a synthetic fusion protein. We linked together a NS3 protease cleavage site to either $NS3^{AI}$ or $NS3^{TI}$, referring to these sequences as StaPL modules (Supplementary Fig. 3a). We then employed $StaPL^{AI}$ and $StaPL^{TI}$ modules to connect a nuclear localization sequence (NLS) to either tandem dimeric YFP (tdYFP) or tandem dimeric RFP (tdRFP). Preservation of each StaPL linkage occurred only with the cognate inhibitor (Supplementary Fig. 3b), and nuclear localization of tdYFP and tdRFP could be controlled independently in the same cells (Supplementary Fig. 4). Thus, orthogonal StaPL-drug pairs enable independent regulation of two proteins.

We next used StaPL sequences to bidirectionally control gene expression. We chose to regulate vascular endothelial growth factor (VEGF), as VEGF upregulation could be beneficial in neuropathy or vascular insufficiency[11], while its downregulation may be useful for wet age-related macular degeneration and cancer[12]. We first expressed in HEK293A cells a synthetic zinc-finger domain targeting the *VEGFA* promoter[13] (ZF^{VEGFA}) fused to either $StaPL^{AI}$ followed by tdYFP and a p65 activation domain, or to $StaPL^{TI}$ followed by

tdRFP and a KRAB repressor domain, testing two substrate sequences within the StaPL modules. As expected, full-length proteins were preserved only in the presence of the cognate drug (Supplementary Fig. 5a). We then tested whether these constructs could mediate pharmacological regulation of endogenous *VEGFA* by quantifying VEGF secreted from transfected cells (Supplementary Fig. 5b). While TPV stabilization of the KRAB-based repressor downregulated VEGF as desired, ASV stabilization of the p65-based activator had unclear effects. We thus replaced p65 with the more potent VP64-p65-Rta (VPR) cassette[14] and reconfirmed drug-dependent protein preservation using the more efficiently cleaved DEMEEC/S substrate (Supplementary Fig. 5a,c). Finally, we tested the ability of the two final constructs, ZF^{VEGFA}-$StaPL^{TI}$-tdRFP-KRAB and ZF^{VEGFA}-$StaPL^{AI}$-YFP-VPR (Supplementary Fig. 6) to regulate *VEGFA* transcription (Fig. 1d). Individually, ZF^{VEGFA}-$StaPL^{TI}$-tdRFP-KRAB decreased VEGF secretion specifically in TPV, while ZF^{VEGFA}-$StaPL^{AI}$-YFP-VPR strongly increased VEGF secretion specifically in ASV. In cells coexpressing both constructs, VEGF was upregulated by ASV and downregulated by TPV, demonstrating orthogonal regulation (Fig. 1d). Thus, StaPL modules can regulate linkage between DNA-binding and regulatory domains in synthetic transcription factors, with two orthogonal StaPL-drug pairs enabling bidirectional control of an endogenous gene.

We then investigated if StaPL modules within internal loops can regulate protein function. We inserted $StaPL^{TI}$ into nuclease-deficient *S. pyogenes* Cas9 (dSpCas9) with an N-terminal fusion to VPR (VPR-dCas9), choosing positions 573 and 1246, within non-conserved loops of dSpCas9. To assay for function, we transfected these constructs and a single guide RNA (sgRNA) targeting a tet operator (tetO) sequence into HEK293 cells stably expressing mCherry from a TRE3G promoter containing 7 tetO repeats[15]. We expected the dSpCas9 domain to be cleaved into non-functional fragments by default, but to retain its ability to fold and function in TPV (Fig. 2a). Both constructs activated RFP expression in TPV, with the variant at 1246 performing better (Supplementary Fig. 7a-b). Cells expressing this protein, VPR-dSpCas9($StaPL^{TI}$) (Supplementary Fig. 8) increased RFP fluorescence 24-fold and RFP mRNA expression 6-fold after 24 h in TPV compared to vehicle (Fig. 2b-c). Thus, intra-domain insertion of a StaPL module enables pharmacological regulation of VPR-dSpCas9 function.

Next, we characterized the kinetics, reversibility, and dose responsiveness of transcriptional activation by StaPL (Supplementary Note 2). Kinetics were consistent with the accumulation of new intact protein copies in the presence of drug (Supplementary Fig. 9a-c). Reversal was not observed 24 h after removal of TPV from VPR-dSpCas9($StaPL^{TI}$) but was observed after removal of ASV from ZF^{VEGFA}-$StaPL^{AI}$-YFP-VPR, consistent with the known covalent mechanism of action of TPV and non-covalent mechanism of action of ASV (Supplementary Fig. 9d-e). Dose responsiveness of VPR-dSpCas9($StaPL^{TI}$) and ZF^{VEGFA}-$StaPL^{AI}$-YFP-VPR mirrored that of $SMASh^{TI}$ and $SMASh^{AI}$, respectively (Supplementary Fig. 9f-g, Supplementary Tables 2-3), indicating consistent drug responsiveness of the $NS3^{TI}$ and $NS3^{AI}$ proteases in different contexts.

Finally, we postulated that StaPL sequences could enable drug-dependent preservation of a tandem dimer. This would allow proteins naturally activated by homodimerization to be activated by NS3 protease inhibitors. We tested this concept on caspase-9 (Casp9), whose

natural activation involves dimerization of an N-terminal domain and which can be artificially activated by chemically induced dimerization[16]. We created a fusion protein consisting of, in order, a minimal Casp9 protease domain, a StaPL^{AI} module, and a second copy of the Casp9 protease domain (Fig. 2d, Supplementary Fig. 10). Stabilization of this tandem dimer, referred to as StaPL-dimerized Casp9 (StaPLd-Casp9), would be expected to cause Casp9 autoactivation and subsequent apoptosis in ASV (Fig. 2d). For testing, we also created a catalytically inactive variant, StaPLd-Casp9^{C287S}. We then expressed these constructs from the same locus in HeLa cells using targeted recombination, with a downstream IRES-RFP cassette as an expresion marker. As expected, cells stably expressing StaPLd-Casp9^{C287S} produced cleaved Casp9 monomer bands in the absence of ASV, but produced full-length protein after 24 h of ASV treatment (Supplementary Fig. 11a). For cells expressing the catalytically active StaPLd-Casp9, we also observed Casp9 monomer bands in the absence of ASV, but immunoblotting of ASV-treated cells failed to detect Casp9, RFP, or the ubiquitous protein β-actin, suggesting cell loss before lysate preparation (Supplementary Fig. 11a). ASV-induced cell death was confirmed by brightfield imaging (Supplementary Fig. 11b), and apoptosis was confirmed by annexin staining and flow cytometry (Supplementary Fig. 11c-d). A fluorescent indicator for the downstream caspase-3 confirmed that StaPLd-Casp9 triggered apoptosis via activation of the caspase cascade (Fig. 2e-f). As expected, dose responsiveness of apoptosis to ASV reflected that of NS3^{AI} inhibition, with maximal apoptosis at 1 μM (Supplementary Fig. 12a-b). Thus, regulation of caspase-9 dimerization by StaPL enables an NS3 protease inhibitor to trigger cell death.

StaPLd-Casp9 shares similarity to iCasp9, a caspase-9 fusion protein activated by dimerizing rapalogs such as AP20187 and which is being tested as a safety switch for cellular therapies such as CAR-T cells[16,17]. StaPLd-Casp9 could have similar applications as iCasp9. We confirmed that StaPLd-Casp9 and iCasp9 were activated specifically by their respective drugs to induce comparable maximum levels of apoptosis after 24 h (Supplementary Fig. 13). The orthogonality of the two systems suggests they could be used to control two populations of cells independently *in vivo*. Since intact copies of StaPLd-Casp9 would need to accumulate in ASV to induce apoptosis, while preexisting copies of iCasp9 should induces apoptosis once a certain concentration of AP20187 is reached, the time course of apoptosis with StaPLd-Casp9 should be more gradual than with iCasp9. Indeed, apoptosis was more gradual with ASV and StaPLd-Casp9 than with AP20187 and iCasp9 (time to maximum effect of 24 h vs 3 h, Supplementary Fig. 14a-b). This suggests the ability to perform partial depletion of a StaPLd-Casp9-expressing cell population by intermittent dosing of ASV, which could be useful for rheostatic control of cellular therapies.

In summary, we describe a generalizable design for drug-inducible proteins in which proteins are rescued from StaPL-induced fragmentation by HCV NS3 protease inhibitors. As examples, we used StaPL modules to confer drug control on protein localization and on the functional output of zinc-finger-based transcriptional regulators. We also demonstrated the ability to regulate a CRISPR/Cas9-based transcriptional activator by internal insertion of a StaPL module, and to regulate apoptosis by linking two copies of caspase-9 with a StaPL module. Potential advantages of StaPL over existing techniques for drug control of protein

function include simplicity, robustness, multiplexibility, and the use of clinically approved drugs (Supplementary Note 3).

We expect that StaPL modules can be used to create drug-stabilized forms of many other natural proteins. For example, loop insertion of StaPL modules could create drug-inducible forms of Cas9 proteins from various species. This will enable two different genes to be targeted by two different sgRNAs and to be regulated by two different drugs, while involving the expression of only two polypeptide chains (for example SpCas9 with a StaPL^{AI} insert and *S. aureus* Cas9 with a StaPL^{TI} insert), compared to four polypeptides when heterodimerizing systems are used[18,19]. More generally, many proteins tolerate the insertion of protein domains into exposed loops[20], and should thus be amenable to drug regulation via internal StaPL module insertion and linkage preservation by NS3 protease inhibitors.

Online Methods

DNA plasmids and molecular cloning

Plasmids were constructed using standard molecular biology techniques: restriction enzyme digest (Fermentas), PCR and overlap extension PCR with PrimeSTAR polymerase (Clontech), and assembly using either In-Fusion enzyme (Clontech) or T4 ligase (Thermo Fisher). DNA was transformed into XL10 Gold (Agilent) or Stellar (Clontech) competent *E. coli* cells with ampicillin (100 μg/mL) selection. Plasmid DNA was isolated with the PureLink hiPure Plasmid Maxiprep Kit (Thermo Fisher) or the Plasmid Plus Midiprep Kit (Qiagen). Subcloned regions were verified by Sanger sequencing, assisted by Geneious software (Biomatters).

Hepatitis C Virus sequences used in this study were derived from genotype 1a HCV (Genbank Accession No. NC_004102). Plasmids encoding PSD95-SMASh, Arc-SMASh, and (Venus) YFP-SMASh mutant variants were under the control of the CMV promoter in the pCMV-SPORT6 backbone (Life Technologies), and were adapted from those described in ref. 10. Plasmids encoding tdYFP-StaPL-NLS and tdRFP-StaPL-NLS, in the pCMV-SPORT6 backbone, consisted of either a tandem pair of Venus YFP connected via a flexible GGSGGS linker (tdYFP) or tdTomato (tdRFP), linked to a StaPL (HCV NS4A-NS3) module with a EDVVCC/H cleavage site in between. A tandem repeat of the SV40 nuclear localization sequence (NLS), with sequence DPKKKRKV, was linked C-terminally to the StaPL via a flexible linker.

Zinc-finger (ZF) plasmids, in the pCMV-SPORT6 backbone, consisted of a ZF DNA binding domain and HA epitope tag, connected to a StaPL module via a DEMEEC/S or EDVVCC/H cleavage site, followed by a fluorescent protein marker (either YFP, tdYFP, or tdRFP), a transcriptional effector (either p65, VPR, or KRAB), and a tandem SV40 nuclear localization sequence (NLS) attached via a DEMEEC/S cleavage site. The human SP1 protein-derived ZF domain architecture targeted a 10-bp region (GGGGAGGATC) beginning eight nucleotides upstream of the transcriptional start site (TSS) of the human *VEGFA* locus, and was previously described by ref. 13. The KRAB repressor consisted of the first 97 residues of the human KOX1 protein. The p65 activator consisted of the last 101

residues of the human NF-κB protein. ZF, p65, and KRAB were synthesized de novo by assembly PCR from oligonucleotides, assisted by the DNAWorks algorithm. VPR activator (VP64-p65-Rta) was amplified from a VPR-dSaCas9 plasmid (a gift from the Stanley Qi lab, Stanford) and its internal NLS was replaced with a GGSGGS linker.

The *S. pyogenes* Cas9 constructs, which carried nuclease-deactivating mutations D10A and H840A (dSpCas9), were under the control of the PGK promoter, and consisted of a VPR transcriptional activator domain linked to BFP, dSpCas9 (with or without a DEMEEC/S cleavage site and StaPLTI module inserted into an internal loop), and a tandem NLS. In these constructs, the VPR's internal NLS was replaced with a GGSGGSGGS linker. These constructs were adapted from a PGK-VPR-BFP-dSpCas9 plasmid which was a gift from the Stanley Qi lab, as was a U6-sgRNA/CMV-GFP plasmid that expressed a *S. pyogenes* single-guide RNA directed to the TRE3G locus (target sequence GTACGTTCTCTATCACTGATA on non-template strand).

Human caspase-9 (excluding its CARD caspase recruitment domain) was amplified from the pET23b-Casp9-His plasmid (a gift from Guy Salvesen lab, Addgene plasmid #11829, ref. 21). Dual copies of the Casp9 large and small subunits were linked together by an HA epitope tag, a DEMEEC/S cleavage site, and a StaPLAI module. This StaPLd-Casp9 construct was subcloned into the pcDNA5/FRT shuttle vector (Thermo Fisher), which contains a CMV promoter. An internal ribosome entry sequence (IRES) and a coding sequence for eqRFP (a monomeric RFP from *Entacmaea quadricolor*) were placed downstream of StaPLd-Casp9. The iCasp9 gene was amplified from the pMSCV-Fdel Casp9.IRES.GFP plasmid (a gift from the David Spencer lab, Addgene plasmid #15567, ref. 16) and subcloned into the IRES:eqRFP-containing pcDNA5/FRT shuttle vector. Catalytic dead variants of StaPLd-Casp9 and iCasp9 were also made by introducing a C287S mutation into each of the large subunits.

Molecular modeling

Manipulation of protein crystal structures was performed using UCSF Chimera (ref. 22) and MacPyMol (Schrödinger). Cocrystals of the HCV NS4A/NS3 protease in complex with asunaprevir (PDB 4WF8, ref. 23) or telaprevir (PDB 3SV6, ref. 24) were modified to include the relevant mutations, and (if applicable) the inhibitor molecule was removed. Structures were then energy minimized in Chimera, and re-imported into MacPyMol for generating images. Modeling of dSpCas9 was performed using a cocrystal of Cas9 and single-guide RNA (PDB 4ZT0, ref. 25).

Cell culture and transfection

HEK293A (Life Technologies) and HeLa (ATCC) were passaged in 100 mm dishes (Falcon) and cultured at 37°C in 5% CO2 in high glucose Dulbecco's modified Eagle's medium (DMEM, Hyclone or Life Technologies) supplemented with 10% (v/v) fetal bovine serum (FBS, Gemini) or 10% calf serum (Gemini), 2 mM glutamine (Gemini), 100 U/mL penicillin, and 100 μg/mL streptomycin (Gemini). Cell cultures were not tested for mycoplasma. For dSpCas9 experiments, monoclonal stable HEK293 cells with a TRE3G-mCherry cassette were used (gift from Stanley Qi lab) and cultured similarly. For HEK293A

and HeLa, transfections were performed with Lipofectamine 2000 or Lipofectamine 3000 (Life Technologies) and Opti-MEM (Life Technologies) according to manufacturer's instructions. For the HEK293-TRE3G-mCherry cell line, either the CalPhos Mammalian Transfection Kit (Clontech) or Lipofectamine 2000 was used. For CalPhos-transfected cells, media was aspirated and replaced with fresh drug-containing media 24 h post-transfection. Negative control transfections were performed using the pCMV-SPORT6 plasmid. For cotransfections with dSpCas9 variants and single guide RNA, DNA amounts were adjusted to produce a 1:1 molar ratio of dSpCas9 plasmid(s) to sgRNA plasmid.

Monoclonal stable HeLa lines expressing StaPLd-Casp9 and iCasp9 constructs were generated via the Flp-In System (Life Technologies). Flp-In T-REx HeLa cells (gift from Stephen Taylor lab, University of Manchester, ref. 26) were initially maintained in DMEM supplemented as described above, and also with 100 μg/mL Zeocin (Thermo Fisher). Transfections occurred in 100-mm dishes in Zeocin-free media. For generating the C287S StaPLd-Casp9 and iCasp9 variant cell lines, cells were cotransfected with the appropriate pcDNA5/FRT shuttle vector and the Flp recombinase expression vector pOG44 (10% shuttle vector, 90% pOG44, by mass). For the wildtype StaPLd-Casp9 and iCasp9 cell lines, cells were also cotransfected with the pcDNA3-XIAP-Myc plasmid (a gift from the Guy Salvesen lab, Addgene plasmid #11833; 10% shuttle vector, 20% pcDNA3-XIAP-Myc, 70% pOG44, by mass). Coexpression of the antiapoptotic protein XIAP was performed to prevent any premature apoptosis due to overexpression of StaPLd-Casp9 or iCasp9. After 48 h, cells were trypsinized with 0.25% Trypsin EDTA solution (Gemini) and replated in 12-well plates (Greiner Bio-One) in DMEM containing 200 μg/mL Hygromycin B (Life Technologies) for selection. Colonies were picked, trypsinized, expanded, and verified by vulnerability to zeomycin, eqRFP fluorescence, HA immunopositivity by western blot, and by extracting genomic DNA (DNeasy Blood and Tissue Kit, Qiagen) for PCR amplification and sequencing confirmation of the inserted Casp9 suicide gene. Downstream experiments were performed in Hygromycin B-containing DMEM.

Chemical reagents

Telaprevir (TPV) and staurosporine (STS) were obtained from AdooQ Biosciences and asunaprevir (ASV) was obtained by custom synthesis (Acme Bioscience). ASV is also commercially available as a research reagent. AP20187 (AP) was purchased from ApexBio. Stocks of each compound were made at 1000× of the final concentration in dimethysulfoxide (DMSO, Santa Cruz Biotechnology) and stored at −20 °C. For experiments with transfected plasmids, ASV and TPV were applied to cells directly prior to transfection, or along with transfection reagents, unless otherwise indicated. Cobalt(II) chloride hexahydrate ($CoCl_2$, Sigma Aldrich) was dissolved in water to make a 400-mM (500×) stock. In applicable experiments, cells were incubated in 800 μM $CoCl_2$ for the final 7 h before harvest, in order to simulate hypoxia.

Antibodies

The following primary antibodies were used for immunoblotting at the indicated dilutions: mouse monoclonal anti-PSD95 (NeuroMab, clone K28/43), 1:1000; rabbit polyclonal anti-β-actin (GeneTex, GTX124214), 1:3333; rabbit polyclonal anti-GAPDH (Santa Cruz,

FL-335/sc-25778), 1:500; rabbit polyclonal anti-Arc (Synaptic Systems, #156 003), 1:200; mouse monoclonal anti-GFP (Pierce, clone GF28R/MA5-15256), 1:1000; rabbit polyclonal anti-tdTomato (OriGene, TA150128), 1:2000; rabbit monoclonal anti-HA (Cell Signaling, C29F4), 1:1000; mouse monoclonal anti-GAPDH (Santa Cruz, clone G-9/sc-365062), 1:500; mouse monoclonal anti-HA (Santa Cruz, clone F-7/sc-7392), 1:1000; rabbit polyclonal anti-eqRFP (Evrogen, AB233), 1:1000; mouse monoclonal anti-β-actin (Santa Cruz, ACTBD11B7/sc-81178), 1:1000. Secondary antibodies were either LI-COR 680RD goat-anti-mouse and 800CW goat-anti-rabbit, or 680RD goat-anti-rabbit and 800CW goat-anti-mouse. Secondaries were used at 1:3333.

Immunoblotting

For SDS-PAGE analysis, cells were cultured in 24- or 12-well plates (Greiner Bio-One) for 8 to 48 h after transfection and drug addition. Culture media were removed, then cells were lysed with 50 or 100 μL of hot (90 °C) SDS lysis buffer (100 mM Tris HCl pH 8.0, 3% SDS, 20% glycerol, 0.2% bromophenol blue, 10% 2-mercaptoethanol). Lysates were sonicated to shear DNA, heated briefly to 90°C, centrifuged, and loaded on either NuPAGE 4-12% Bis-Tris (Life Technologies) or 4-15% Criterion TGX (Bio-Rad) gels, along with Novex Sharp pre-stained protein standard (Life Technologies). Transfers onto PVDF membrane were performed using either the iBlot system (Life Technologies) or the Trans-Blot Turbo system (Bio-Rad).

Membranes were typically probed with primary and secondary antibodies using the iBind system (Life Technologies). Alternatively, immunoprobing was done by blocking the membrane with 7.5% (w/v) nonfat dry milk in Tris-buffered saline (TBS) for 1 h at ambient temperature on an electric rocker, washing three times using TBS with 0.1% Tween 20 (TBS-T), incubating 1 h with primary antibodies in 5% bovine serum albumin (BSA) in TBS-T, washing three times in TBS-T, incubating 1 h with fluorescent secondary antibodies in 7.5% nonfat dry milk in TBS-T, and washing three times in TBS-T.

For the immunoblotting experiment depicted in Supplementary Fig. 1b, membranes were cut into two sections and truncated in order to stain all PSD95 sections in parallel with mouse anti-PSD95, and all GAPDH sections in parallel with rabbit anti-GAPDH. In all other cases, membranes were stained intact. Immunoblot membranes were scanned using an Odyssey or CLx imager (LI-COR). Membrane scans were cropped in order to generate figures. For non-truncated immunoblot membranes, uncropped versions have been made available (Supplementary Fig. 15).

Western blot quantifications were performed using the Fiji distribution of ImageJ (ref. 27). Integrated densities for bands of the same protein species were measured using a consistently sized rectangle, and background measurements from the same lane were subtracted from these values. Protein of interest bands were normalized via dividing by loading control bands, which were quantified by the same method. Data analysis was performed using Excel (Microsoft) and OpenOffice (Apache) software.

Microscopy

Brightfield microscopy of live StaPLd-Casp9-expressing HeLa cells (in 12-well plates, Greiner Bio-One) was performed on an EVOS FL Cell Imaging System with a 4× 0.1-numerical aperture (NA) air objective. Fluorescence widefield microscopy of live transfected HeLa cells (in 35 mm glass bottom 4-chamber dishes, In Vitro Scientific), live or fixed transfected TRE3G-mCherry stable HEK293 cells (in plastic 12-well plates, Greiner Bio-One, or glass bottom 12-well plates, In Vitro Scientific, respectively), and stained/fixed StaPLd-Casp9-expressing HeLa cells (mounted on glass slides with #1.5 cover glass) was performed on an Axiovert 200M inverted microscope (Zeiss) with a 40× 1.2-NA water immersion, 5× 0.25-NA air, or 10× 0.5-NA air objective, respectively. The following excitation (ex) and emission (em) filters were used: Green/Yellow (YFP, Alexa 488), ex 485/10 nm (Chroma), em 510 nm longpass dichroic (Omega) and 525/40 nm (Chroma); Red (RFP, eqRFP), ex 568/20 nm (Omega), em 585 longpass dichroic (Chroma) and 620/60 nm (Chroma). Excitation was from an X-Cite 120-W metal-halide lamp with a 3-mm-core liquid light guide (Lumen Dynamics) and acquisition was performed by an ORCA-ER camera (Hamamatsu). The system was controlled by a MacBook Pro computer (A1261, Apple) running the MacOS 10.6.8 operating system (Apple) and Micro-Manager 1.4.10 software (ref. 28).

Confocal fluorescence microscopy of live transfected HEK293A cells was performed in 35-mm glass-bottom 4-chamber dishes (In Vitro Scientific) on an UltraVIEW VoX system (PerkinElmer) equipped with a CSU-X1 spinning disc (Yokogawa Electric) and a C9100-50 EM-CCD camera (Hamamatsu), controlled by Volocity 5 software (Improvision). Imaging was performed with an Apochromat 63× 1.4-NA oil immersion objective (Zeiss). The following excitation (ex) lasers (at 30% power) and emission (em) filters were used: YFP, ex 488 nm laser, em 525/50 nm; RFP, ex 561 nm laser, em 615/70 nm.

Plastic 12-well plates or glass bottom cell culture vessels for HEK293/HEK293A cells were typically coated with 0.5 mg/mL poly-D-lysine hydrobromide (Sigma-Aldrich) in water by incubating at 37 °C for 4 h to overnight, and were washed four times with water prior to plating cells. Live StaPLd-Casp9 HeLa cells were imaged in DMEM supplemented as described above, and live transfected HeLa cells and HEK293-TRE3G-mCherry cells were imaged in Hank’s Balanced Salt Solution (HBSS, Hyclone). In the case of time course experiments, appropriate protease inhibitor drug was maintained in HBSS during imaging, before returning cells to fresh drug-containing DMEM. Live transfected HEK293A cells were imaged in FluoroBrite DMEM (Life Technologies) supplemented as described above. Fixed cells were fixed using 4% paraformaldehyde (Electron Microscopy Sciences) in phospho-buffered saline (PBS, HyClone) for 15 min at ambient temperature, washed twice with HBSS, and subsequently stored in HBSS.

Image processing and analysis was performed with Fiji. For stained/fixed StaPLd-Casp9-expressing HeLa cells, 10-μm-tall z-stacks were acquired in 1-μm intervals and were subsequently transformed into maximum intensity projections and background-subtracted. For live transfected HEK293A cells, z-stacks were acquired in 0.5-μm intervals and ranges encompassing 4 μm were transformed into maximum intensity projections. For live or fixed

transfected HEK293-TRE3G-mCherry cells, background-subtracted images were quantified for RFP fluorescence using the integrated density function.

Enzyme-linked immunosorbent assay (ELISA)

HEK293A cells were cultured in 12-well plates (Greiner Bio-One) with 1 mL of DMEM (supplemented as previously described) in each well, and were transfected 48 h prior to harvesting media supernatants (transfection reagent volume, 200 μL). Media were not changed after transfection. Appropriate protease inhibitor drugs were applied concurrent with transfection. Cells transfected with empty vector and given identical protease inhibitor treatments served as controls. From each well, 900 μL of media supernatant was collected for ELISA analysis, and frozen at −20 °C until it was processed. Samples were thawed to ambient temperature one hour before use, and cleared by centrifuging at 10,000g for 10 min at 4 °C.

Sandwich ELISA was performed using the Human VEGF Quantikine ELISA Kit (R&D Systems) according to manufacturer's protocol. Absorbances at 450 nm (with reference wavelength 540 nm) were measured thrice and averaged, using a Infinite M1000 PRO plate reader (Tecan) under the control of i-control software (Tecan). Human VEGF protein dilution standards were used to calculate sample [VEGF] values by 4-parameter logistic regression (www.elisaanalysis.com). In some cases, sample measurements exceeded those of the top standard value, and were diluted two-fold and rescanned in order to interpolate them. The calculated [VEGF] for such samples was thus multiplied by two. Since each well of HEK293A contained 1.2 mL of media post-transfection, [VEGF] values were adjusted by a factor of 1.2 to obtain true concentrations in pg/mL. VEGF measurements are expressed as differences from cells transfected with empty vector and incubated in similar drug conditions.

Quantitative real-time PCR

To measure mRNA levels in HEK293A or HEK293-TRE3G-mCherry cells, cells were first plated on plastic 12-well plates (Greiner Bio-One or Thermo Scientific Nunclon Delta Surface). For HEK293-TRE3G-mCherry cells, plates were coated with 0.5 mg/mL poly-D-lysine hydrobromide (Sigma-Aldrich) in water by incubating at 37 °C for 4 h to overnight, and were washed four times with water prior to plating. Cells were harvested by aspirating media and lysing with 500 μl of RNA lysis buffer (Zymo). Lysates were frozen at −20 °C prior to processing 150 μl of each sample with molecular biology grade ethanol (Sigma) and the Quick-RNA Microprep Kit (Zymo), which incorporates a DNase digestion step. Extracted RNAs were verified by to have 260/230 and 260/280 ratios of >1.8 using a NanoDrop spectrophotometer (Thermo Fisher); otherwise they were re-extracted.

RNAs were reverse transcribed using Superscript IV VILO Master Mix (Thermo Fisher) according to manufacturer's instructions. Prior to reverse transcription, concentrations of RNA samples were normalized by diluting some with RNase-free water. Each RNA sample was reverse transcribed in duplicate. cDNAs were used as templates in PCR reactions using the Applied Biosystems Taqman Gene Expression Master Mix (Fisher Scientific). PCR reactions (10 μl) were performed in Hard-Shell thin wall 384-well PCR plates (Bio-Rad)

sealed with Microseal B adhesive (Bio-Rad) and were analyzed on a Bio-Rad CFX384 thermocycler. Each PCR reaction for a given cDNA sample was performed in duplicate. All steps were performed using barrier pipette tips.

PCR primers and Taqman probes were synthesized by Integrated DNA Technologies, and used at final concentrations of 500 nM for primers and 250 nM for probes. Sequences of primer pairs and probes were as follows:

mCherry RFP forward primer, GAGGCTGAAGCTGAAGGAC

mCherry RFP reverse primer, GATGGTGTAGTCCTCGTTGTG

mCherry RFP probe, 56-FAM/CCAACTTGA/ZEN/TGTTGACGTTGTAGGCG/3IABkFQ

Human *VEGFA* forward primer, CCATGAACTTTCTGCTGTCTTG

Human *VEGFA* reverse primer (exon-spanning), TGAACTTCACCACTTCGTGAT

Human *VEGFA* probe, 56-FAM/TGCTCTACC/ZEN/TCCACCATGCCAAG/3IABkFQ

Human *GAPDH* forward primer, CCATGTTCGTCATGGGTGTGA

Human *GAPDH* forward primer (exon-spanning), CATGGACTGTGGTCATGAGT

Human *GAPDH* probe, 56-FAM/TCCTGCACC/ZEN/ACCAACTGCTTAGCA/3IABkFQ.

Using dilution series, primer/probe sets were verified to have efficiencies of > 90%, and pairs of primer/probe sets (RFP & GAPDH, VEGFA & GAPDH) were verified to have efficiencies within 5% of one another. Cq values were calculated from amplification curves using the Single Threshold method in CFX Manager software (Bio-Rad). Data were analyzed in Excel. Relative gene expression values were obtained by the ddCq method: first, Cq values for genes of interest were normalized by the housekeeping gene GAPDH, and then, the resultant values were normalized to drug- and/or time-matched empty vector-transfected controls.

Cell staining

To assess the activity of engineered suicide genes, StaPLd-Casp9-expressing or iCasp9-expressing HeLa cells were stained after drug incubation. Media were collected to harvest dead/lifted cells, adherent cells were trypsinized to harvest living cells, and the two were pooled and pelleted at 500g for 5 min. Cells were washed once with HBSS, resuspended in either HBSS or Annexin V Binding Buffer (Biotium), and stained with the NucView 488 Caspase-3 Assay Kit for Live Cells (Biotium) or the Annexin V CF488A Conjugate kit (Biotium), respectively, according to manufacturer's instructions. In some instances, cells of the parent cell line (Flp-In HeLa) were annexin V-stained in parallel. For medium-term preservation, cells were fixed in 4% PFA in PBS for 15 min at ambient temperature following staining, centrifuged at 10,000g, and resuspended in HBSS after aspirating the PFA. For microscopy, a 25 μL droplet of each sample was then placed on a Superfrost Plus glass slide (Fisher Scientific), and allowed to dry partially, before adding Vectashield

Mounting Medium with DAPI (Vector Labs) and a #1.5 cover glass (Fisher Scientific). Slides were sealed with clear nail polish and kept at 4 °C.

Flow cytometry

Flow cytometry was performed on live or fixed cells (for annexin V-stained cells) or fixed cells (for the caspase-3 sensor) prepared as above, using a Digital Vantage instrument (Becton Dickinson) under the control of CellQuest software (Becton Dickinson), operated by the Stanford Shared FACS Facility. A 488-nm laser was used to excite Alexa 488 stain and a 594-nm laser was used to excite eqRFP. The parent Flp-In HeLa cell line, which did not express eqRFP, assisted in confirming eqRFP-positive monoclonal populations for the stable cell lines. For each sample, 10^4 events were collected. Gates were constructed inside forward scatter and side scatter plots (FSC-A vs. SSC-A and FSC-H vs. FSC-A) to exclude debris and non-singlet events, respectively (Supplementary Fig. 11c). Cytometry data was analyzed and processed using FlowJo software (FlowJo LLC).

Statistical analyses

Statistical analyses were performed using Excel (Microsoft) and Prism (Graphpad). To test for significant pairwise differences between drug responsiveness of $SMASh^{WT}$, $SMASh^{AI}$, and $SMASh^{TI}$ variants for a given ASV or TPV drug concentration, normality of the data were confirmed by the Shapiro-Wilk normality test, then data were subjected to two-way ANOVA, with multiple comparisons between each variant's mean normalized NS3 activity for each concentration of ASV and TPV. Data for ASV and TPV were analyzed separately. P values from multiple comparisons were corrected post hoc by Tukey test. Corrected P values are as follows:

µM ASV: $NS3^{wt}$ vs. $NS3^{AI}$, P = 0.2476; $NS3^{wt}$ vs. $NS3^{TI}$, P = 0.9568; $NS3^{AI}$ vs. $NS3^{TI}$, P = 0.1530

0.1 µM ASV: $NS3^{wt}$ vs. $NS3^{AI}$, P = 0.1404; $NS3^{wt}$ vs. $NS3^{TI}$, P = 0.0017; $NS3^{AI}$ vs. $NS3^{TI}$, P = <0.0001

1 µM ASV: $NS3^{wt}$ vs. $NS3^{AI}$, P = >0.9999; $NS3^{wt}$ vs. $NS3^{TI}$, P = <0.0001; $NS3^{AI}$ vs. $NS3^{TI}$, P = <0.0001

10 µM ASV: $NS3^{wt}$ vs. $NS3^{AI}$, P = 0.9063; $NS3^{wt}$ vs. $NS3^{TI}$, P = 0.0001; $NS3^{AI}$ vs. $NS3^{TI}$, P = <0.0001

µM TPV: $NS3^{wt}$ vs. $NS3^{AI}$, P = 0.9174; $NS3^{wt}$ vs. $NS3^{TI}$, P = 0.2797; $NS3^{AI}$ vs. $NS3^{TI}$, P = 0.4779

1 µM TPV: $NS3^{wt}$ vs. $NS3^{AI}$, P = 0.3484; $NS3^{wt}$ vs. $NS3^{TI}$, P = 0.0088; $NS3^{AI}$ vs. $NS3^{TI}$, P = 0.1513

10 µM TPV: $NS3^{wt}$ vs. $NS3^{AI}$, P = 0.2116; $NS3^{wt}$ vs. $NS3^{TI}$, P = 0.0088; $NS3^{AI}$ vs. $NS3^{TI}$, P = 0.0002

To test for significant pairwise differences between VEGF secretion in different drug conditions for a given zinc-finger construct or constructs, normality of the data were confirmed by the Shapiro-Wilk normality test, then data were subjected to one-way

ANOVA, with multiple comparisons between mean normalized VEGF concentration for each drug condition. Data for each expressed zinc-finger construct or constructs were analyzed separately. P values from multiple comparisons were corrected post hoc by Tukey test. Corrected P values are as follows:

ZF^{VEGFA}-$StaPL^{TI}$-tdRFP-KRAB: DMSO vs. ASV, P = 0.9969

ZF^{VEGFA}-$StaPL^{TI}$-tdRFP-KRAB: DMSO vs. TPV, P = 0.0009

ZF^{VEGFA}-$StaPL^{TI}$-tdRFP-KRAB: ASV vs. TPV, P = 0.0009

ZF^{VEGFA}-$StaPL^{AI}$-YFP-VP: DMSO vs. ASV, P = 0.0002

ZF^{VEGFA}-$StaPL^{AI}$-YFP-VPR: DMSO vs. TPV, P = 0.9596

ZF^{VEGFA}-$StaPL^{AI}$-YFP-VPR: ASV vs. TPV, P = 0.0003

ZF^{VEGFA}-$StaPL^{TI}$-tdRFP-KRAB + ZF^{VEGFA}-$StaPL^{AI}$-YFP-VPR: DMSO vs. ASV, P = 0.0018

ZF^{VEGFA}-$StaPL^{TI}$-tdRFP-KRAB + ZF^{VEGFA}-$StaPL^{AI}$-YFP-VPR: DMSO vs. TPV, P = 0.2624

ZF^{VEGFA}-$StaPL^{TI}$-tdRFP-KRAB + ZF^{VEGFA}-$StaPL^{AI}$-YFP-VPR: ASV vs. TPV, P = 0.0005

Data Availability

Datasets supporting the findings of the current study are available from the corresponding author upon request.

Accession Codes

Mammalian expression plasmids with complete sequence information are available at addgene.org for YFP-$SMASh^{AI}$ (111500), YFP-$SMASh^{TI}$ (111501), ZF^{VEGFA}-$StaPL^{AI}$-YFP-VPR (111502), ZF^{VEGFA}-$StaPL^{TI}$-tdRFP-KRAB (111504), VPR-dSpCas9($StaPL^{TI}$) (111508), and StaPLd-Casp9 (111511).

Supplementary Material

Refer to Web version on PubMed Central for supplementary material.

Acknowledgments

We thank T. Knaak and the Stanford Shared FACS Facility for their assistance with flow cytometry experiments and the M. Kay lab for usage of their real-time thermocycler. We are grateful to L.S. Qi, A. Straight (Stanford), D. Spencer (Baylor College of Med.). and G. Salvesen (Sanford Burnham Inst.) for providing cell lines and plasmids. We also wish to thank V. Duong, Y. Geng, X. Zhou, H. Chung, L. Ning, Y. Yang, and other members of the Lin Lab for advice and helpful discussions, and we thank S. Dixon for feedback. This work was supported by a Stanford Graduate Fellowship and NSF Graduate Research Fellowship (C.L.J.), a Stanford Bio-X Undergraduate Summer Research grant and Stanford UAR Major grant (R.K.B.), and a NIH/NIGMS EUREKA grant 5R01GM098734 (M.Z.L.).

References

1. Picard D. Posttranslational regulation of proteins by fusions to steroid-binding domains. Methods Enzymol. 2000
2. Rakhit R, Navarro R, Wandless TJ. Chemical biology strategies for posttranslational control of protein function. Chem Biol. 21:1238–1252.2014; [PubMed: 25237866]
3. Armstrong CM, Goldberg DE. An FKBP destabilization domain modulates protein levels in Plasmodium falciparum. Nat Methods. 4:1007–1009.2007; [PubMed: 17994030]
4. Liu YC, Singh U. Destabilization domain approach adapted for regulated protein expression in the protozoan parasite Entamoeba histolytica. Int J Parasitol. 44:729–735.2014; [PubMed: 24929134]
5. Gray DC, Mahrus S, Wells JA. Activation of specific apoptotic caspases with an engineered small-molecule-activated protease. Cell. 142:637–646.2010; [PubMed: 20723762]
6. Zetsche B, Volz SE, Zhang F. A split-Cas9 architecture for inducible genome editing and transcription modulation. Nat Biotechnol. 33:139–142.2015; [PubMed: 25643054]
7. McCauley JA, Rudd MT. Hepatitis C virus NS3/4a protease inhibitors. Curr Opin Pharmacol. 30:84–92.2016; [PubMed: 27544488]
8. Butko MT, et al. Fluorescent and photo-oxidizing TimeSTAMP tags track protein fates in light and electron microscopy. Nat Neurosci. 15:1742–1751.2012; [PubMed: 23103964]
9. Lin MZ, Glenn JS, Tsien RY. A drug-controllable tag for visualizing newly synthesized proteins in cells and whole animals. Proc Natl Acad Sci U S A. 105:7744–7749.2008; [PubMed: 18511556]
10. Chung HK, et al. Tunable and reversible drug control of protein production via a self-excising degron. Nat Chem Biol. 11:713–720.2015; [PubMed: 26214256]
11. Giacca M, Zacchigna S. VEGF gene therapy: therapeutic angiogenesis in the clinic and beyond. Gene Ther. 19:622–629.2012; [PubMed: 22378343]
12. Ferrara N, Adamis AP. Ten years of anti-vascular endothelial growth factor therapy. Nat Rev Drug Discov. 15:385–403.2016; [PubMed: 26775688]
13. Liu PQ, et al. Regulation of an endogenous locus using a panel of designed zinc finger proteins targeted to accessible chromatin regions. Activation of vascular endothelial growth factor A. J Biol Chem. 276:11323–11334.2001; [PubMed: 11145970]
14. Chavez A, et al. Highly efficient Cas9-mediated transcriptional programming. Nat Methods. 12:326–328.2015; [PubMed: 25730490]
15. Zhou XX, et al. A Single-Chain Photoswitchable CRISPR-Cas9 Architecture for Light-Inducible Gene Editing and Transcription. ACS Chem Biol. 13:443–448.2018; [PubMed: 28938067]
16. Straathof KC, et al. An inducible caspase 9 safety switch for T-cell therapy. Blood. 105:4247–4254.2005; [PubMed: 15728125]
17. Gargett T, Brown MP. The inducible caspase-9 suicide gene system as a “safety switch” to limit on-target, off-tumor toxicities of chimeric antigen receptor T cells. Front Pharmacol. 5:235.2014; [PubMed: 25389405]
18. Gao Y, et al. Complex transcriptional modulation with orthogonal and inducible dCas9 regulators. Nat Methods. 13:1043–1049.2016; [PubMed: 27776111]
19. Pu J, Kentala K, Dickinson BC. Multidimensional Control of Cas9 by Evolved RNA Polymerase-Based Biosensors. ACS Chem Biol. 13:431–437.2018; [PubMed: 28809467]
20. Heinis C, Johnsson K. Using peptide loop insertion mutagenesis for the evolution of proteins. Methods Mol Biol. 634:217–232.2010; [PubMed: 20676987]
21. Stennicke HR, et al. Caspase-9 can be activated without proteolytic processing. J Biol Chem. 274:8359–8362.1999; [PubMed: 10085063]
22. Yang Z, et al. UCSF Chimera, MODELLER, and IMP: an integrated modeling system. J Struct Biol. 179:269–278.2012; [PubMed: 21963794]
23. Soumana DI, Ali A, Schiffer CA. Structural analysis of asunaprevir resistance in HCV NS3/4A protease. ACS Chem Biol. 9:2485–2490.2014; [PubMed: 25243902]
24. Romano KP, et al. The molecular basis of drug resistance against hepatitis C virus NS3/4A protease inhibitors. PLoS Pathog. 8:e1002832.2012; [PubMed: 22910833]

25. Jiang F, Zhou K, Ma L, Gressel S, Doudna JA. A Cas9-guide RNA complex preorganized for target DNA recognition. Science. 348:1477–1481.2015; [PubMed: 26113724]

26. Tighe A, Staples O, Taylor S. Mps1 kinase activity restrains anaphase during an unperturbed mitosis and targets Mad2 to kinetochores. J Cell Biol. 181:893–901.2008; [PubMed: 18541701]

27. Schindelin J, et al. Fiji: an open-source platform for biological-image analysis. Nat Methods. 9:676–682.2012; [PubMed: 22743772]

28. Edelstein AD, et al. Advanced methods of microscope control using μManager software. J Biol Methods. 12014;

Editor's Summary

Stabilizable polypeptide linkages (StaPLs) based on hepatitis C virus protease enable robust, reversible, and orthogonal chemogenetic control of protein functions, including CRISPR/Cas9 activity, transcription, and protein dimerization.

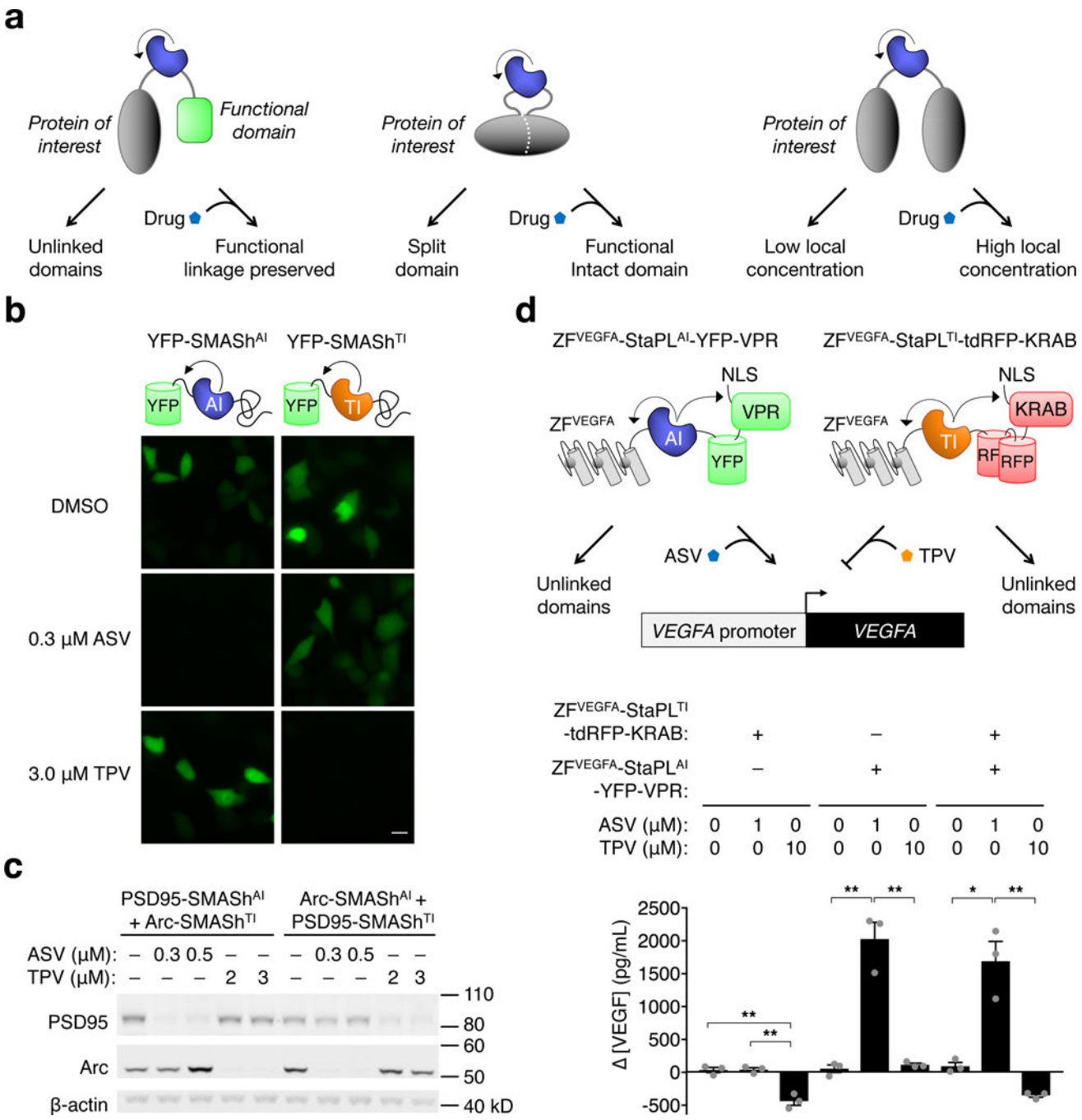

Figure 1.

StaPL concept and engineering of orthogonal NS3 proteases and StaPL effectors. **(a)** A StaPL module, comprising HCV NS3 protease and a cognate substrate sequence linked in cis, can be used to link two functional domains in an artificial multidomain protein (left), to connect two fragments of a natural protein domain (center), or to connect two copies of a protein as a tandem dimer (right). **(b)** Proteases $NS3^{AI}$ (asunaprevir inhibited) and $NS3^{TI}$ (telaprevir inhibited) allow orthogonal drug-induced degradation of YFP via preservation of degron-containing SMASh tag in live Hela cells 24 h after transfection and drug addition.

Scale bar, 20 μm. Data represent a single experiment. Corroborating results were obtained in an independent immunoblot experiment (data not shown). **(c)** SMASh tagging of PSD95 and Arc can be controlled independently in the same cells via orthogonal tags. HeLa cells were lysed 24 h after transfection and drug treatment for immunoblotting. Data represent a single experiment. **(d)** Orthogonal StaPL modules allow bidirectional transcriptional control via synthetic transcription factors. Top, designs of ZF^{VEGFA}-$StaPL^{AI}$-YFP-VPR and ZF^{VEGFA}-$StaPL^{TI}$-tdRFP-KRAB. Bottom, bidirectional regulation of VEGF production by ZF^{VEGFA}-$StaPL^{AI}$-YFP-VPR and ZF^{VEGFA}-$StaPL^{TI}$-tdRFP-KRAB. 48 h after HEK293A transfection and treatment with DMSO, ASV, or TPV, VEGF in culture media was quantified by ELISA. Mean values from 3 independent experiments are graphed. Concentrations were calculated relative to similarly treated cells transfected with empty vector. (Mean empty vector values were 716 pg/mL for DMSO, 673 pg/mL for ASV, and 930 pg/mL for TPV). Grey dots, values from the individual experiments. Error bars, s.e.m. For pairwise comparisons, *P < .01, **P < .001 by 1-way ANOVA (see Online Methods for P values).

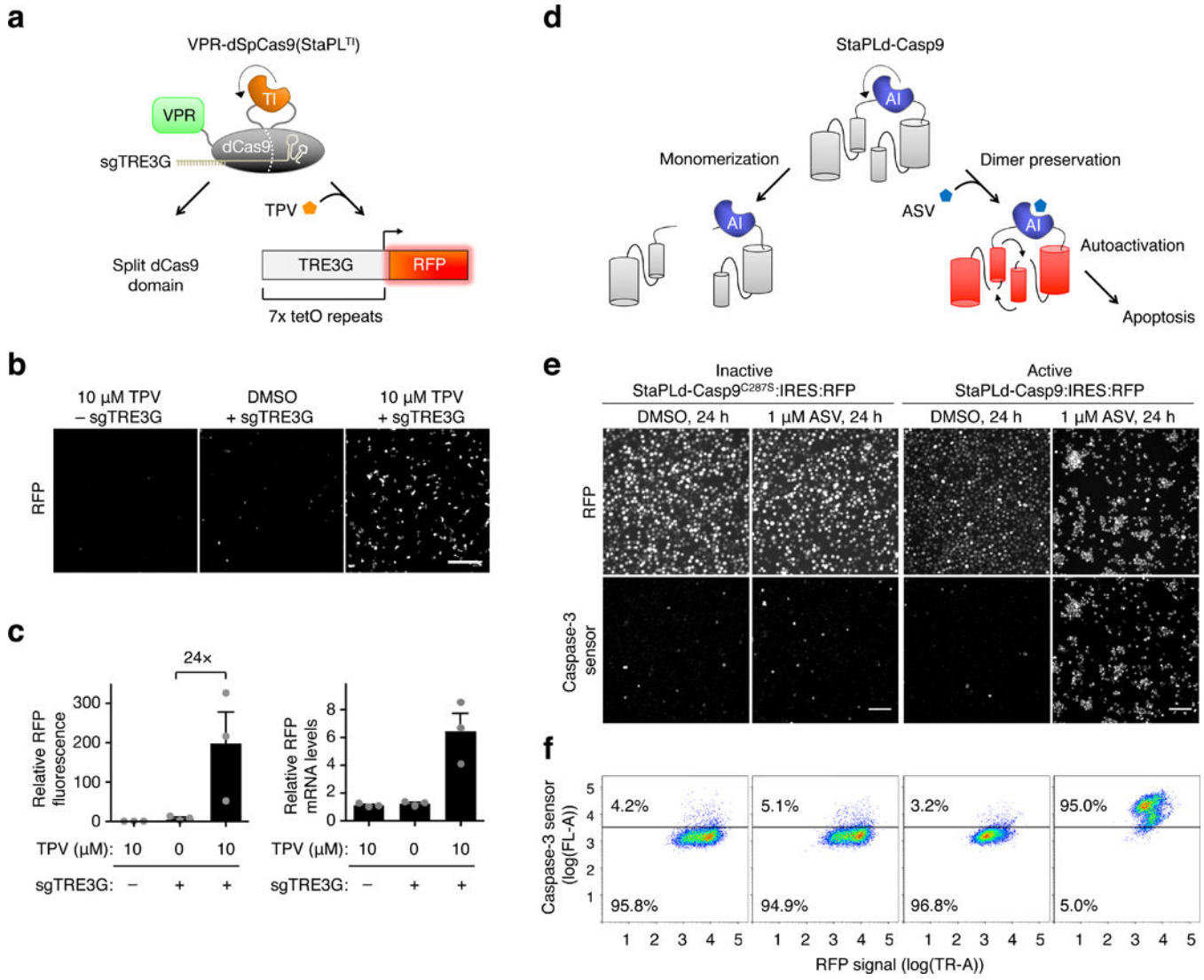

Figure 2.

Applications of StaPL modules to preserving protein folding and inducing protein dimerization. **(a)** Schematic of a single-chain TPV-stabilized SpCas9-based transcriptional activator, VPR-dSpCas9(StaPL^{TI}). **(b)** VPR-dSpCas9(StaPL^{TI}) activated an mCherry RFP reporter gene in the presence of sgRNA and TPV. Live HEK293-TRE3G-mCherry cells were imaged 48 h after transfection. Representative data from 3 independent experiments. Scale bar, 200 μm. **(c)** Efficacy of VPR-dSpCas9(StaPL^{TI}). Left, mean RFP fluorescence from 3 independent experiments; at least 7 fields were imaged per condition in each experiment. Cells were imaged 48 h after transfection. Right, mean RFP gene activation as measured by RT-qPCR from 3 independent experiments. Cells were lysed 48 h after transfection. All values were normalized to drug-matched cells transfected with empty vector alone. Error bars, s.e.m. **(d)** Schematic of StaPLd-Casp9, in which caspase-9 is activated by chemical preservation of a tandem dimer formed via a StaPL^{AI} module. **(e)** Staining with a caspase-3 sensor confirms caspase cascade activation by ASV. HeLa cells expressing StaPLd-Casp9:IRES:RFP or inactive (C287S) control were incubated 24 h in

drug, then stained, fixed, and imaged. RFP expression serves as a marker for StaPLd-Casp9 expression. For RFP panels of active StaPLd-Casp9 cells, intensity is scaled twofold tighter than for the inactive StaPLd-Casp9 cells. Scale bars, 100 μm. **(f)** Fixed cells stained with caspase-3 sensor were analyzed by flow cytometry, confirming caspase-3 activation in ASV-treated cells expressing StaPLd-Casp9, but not cells expressing StaPLd-Casp9^{C287S}. Panels (e) and (f) represent a single experiment.